Macromolecules
ARTICLE

Macromolecules **2010**, *43*, 7689–7694 **7689**
DOI: 10.1021/ma101035h

Coupling between Crystal Melting and Rigid Amorphous Fraction Mobilization in Poly(ethylene terephthalate)

Maria Laura Di Lorenzo,*,† Maria Cristina Righetti,‡ Mariacristina Cocca,† and Bernhard Wunderlich§

†*Istituto di Chimica e Tecnologia dei Polimeri (CNR), c/o Comprensorio Olivetti, Via Campi Flegrei, 34,80078 Pozzuoli (NA), Italy,* ‡*Istituto per i Processi Chimico-Fisici (CNR), Area della Ricerca, Via G. Moruzzi, 1, 56124 Pisa, Italy, and* §*Department of Chemistry, The University of Tennessee, Knoxville, Tennessee 37996, and Rensselaer Polytechnic Institute, Troy, New York 12180*

Received May 10, 2010; Revised Manuscript Received August 4, 2010

ABSTRACT: A thorough analysis of the melting behavior of poly(ethylene terephthalate) (PET) is detailed in this contribution. Isothermal crystallization at 190 °C followed by cooling to room temperature provides a three-phase structure composed of a mobile amorphous, a crystalline, and a rigid amorphous fraction. A close connection between multiple melting and devitrification of the rigid amorphous fraction in PET is revealed by conventional and temperature-modulated calorimetry. Rearrangements of PET crystals at high temperatures involve recrystallization/annealing/crystal perfection following partial melting, which can occur only if the amorphous chain portions coupled to the crystal/melt phase boundary have sufficient mobility. Such mobility can be achieved above the glass transition of the amorphous chain segments coupled with the just-melted crystals. Combined analysis of the reversing heat capacity monitored during quasi-isothermal modulation with the thermal properties of the resulting structure suggests that annealing at temperatures below 210 °C does not result in considerable reorganization and perfection of the crystal phase. The temperature of 210 °C seems to be the point at which the rigid amorphous fraction coupled with the crystal phase attains sufficient mobility to allow development of crystals with increased perfection and thus higher thermal stability.

Introduction

Fusion of semicrystalline polymers is a complex phase transition due to the metastability of their structure. A number of such semicrystalline polymers exhibit double or multiple melting upon heating in differential scanning calorimetry (DSC).[1−12] This behavior is closely linked to the thermal history of the material. Its origin can be ascribed to a variety of sources like the presence of various crystal modifications, molecular weight segregation that had accompanied crystallization, variations in morphology, orientation effects, or melting, recrystallization and annealing taking place during analysis.[1]

Poly(ethylene terephthalate) (PET) is a typical polymer with such complex melting behavior. On heating, it can show three main fusion endotherms with sizes and positions related to its thermal history.[1] The temperatures of all of these peaks were recently linked by fast scanning calorimetry (FSC) to annealing and recrystallization having occurred subsequent to the crystallization.[13] In isothermally crystallized samples, a small endotherm (sometimes called an "annealing peak") is often observed during heating about 10−30 °C above the crystallization temperature.[14] This small thermal event not only is seen in PET but also has been detected in a number of other polymers, including poly(phenylene sulfide) (PPS),[15] isotactic polystyrene,[16] nylon-6,[17] bisphenol A polycarbonate,[6,18] poly(3-hydroxybutyrate),[18] etc., but its nature is still under debate for some of these polymers. Several authors associate it to melting of secondary or more defective crystals;[5,8] others link it to enthalpy recovery of the rigid amorphous fraction (RAF),[14−16] which consists of amorphous chain portions whose mobility is hindered by the crystalline structures they are attached to and whose thermal properties are still not studied in detail for the majority of semicrystalline polymers.

Experimental data on vitrification and devitrification of the rigid amorphous fraction of semicrystalline polymers are not easy to obtain by calorimetry. Often contradictory results appear in the literature. This disagreement arises from the intrinsic nanophase structure of the RAF which is made of amorphous chain segments coupled with crystal portions across phase boundaries. This leads to differently structured layers of molecular segments, which, due to the small volume of the nanophases, usually result in a broad devitrification range, not easily detectable by calorimetry. In addition, the mobilization of the rigid amorphous fraction often overlaps melting of the coupled crystals, so that quantitative determination of mobility of the amorphous chain portion in the temperature range between the glass transition of the MAF and crystal melting is difficult by DSC, except in cases where the two thermal events take place in sufficiently separated temperature ranges.[19−21]

Some attempts to investigate a link between crystal melting and devitrification of the RAF in poly(ethylene terephthalate) appeared in the literature. Cebe et al. suggested that, for PET crystallized stepwise under quasi-isothermal cooling, the RAF devitrifies before the start of melting, at least on quasi-isothermal heating.[22] A similar hypothesis was put forward also in ref 23, again on the basis of quasi-isothermal step analysis of PET, but crystallized during continuous cooling at 5 °C/min. There, however, it was also pointed out that the temperature at which the reversing heat capacities reaches the value expected for full devitrification of the RAF "is sufficiently close to the beginning

*Corresponding author: e-mail dilorenzo@ictp.cnr.it; Ph +39-081-867.5059; Fax +39-081-867.5230.

Published on Web 08/25/2010

of melting that the actual crossover temperature may be somewhat higher due to some low temperature reversible melting."[23]

The occurrence of mobilization of the rigid amorphous fraction in the melting range of PET was, instead, postulated by other authors. According to Schick and co-workers, PET crystals must melt before the amorphous chain segments that constitute the RAF can become mobile.[24] No separate glass transition for RAF was detected by DSC before melting of the crystals, and no significant differences of relaxation strength of dielectric and dynamic mechanical spectroscopy were observed for differently crystallized PET samples, so that devitrification of RAF was judged not to occur before the start of melting. Song claimed, on the basis of temperature-modulated DSC (TMDSC), that the reversing heat flow profiles and their first derivatives of isothermally crystallized PET can be interpreted as devitrification of the rigid amorphous fraction that takes place parallel with the first apparent endotherm that appears several degrees above the crystallization temperature; i.e., low-temperature melting in PET mainly results from the transition of the rigid amorphous fraction accompanied by some enthalpy relaxation that causes the nonreversing thermal event.[14] Righetti et al., instead, demonstrated that in PET multiple processes, involving both the crystalline and the rigid amorphous fraction, overlap in the temperature range in which the low-temperature endotherm is observed.[25] This small endotherm therefore results from the latent heat associated with melting of a small crystal population plus the enthalpy recovery that accompanies partial mobilization of the rigid amorphous fraction. This conclusion was drawn on the basis of a new procedure of analysis of TMDSC data which consists of the analysis of the initial points of the steady-state heat-flow-rate signals in the heating and cooling semiperiods with the temperature modulation being performed with a sawtooth profile.[25]

Summarizing, on the basis of calorimetric data, some authors claim that in PET the rigid amorphous fraction mobilizes, at least in part, in the temperature range where fusion of the crystals occurs; others assert that all amorphous segments are fully mobilized before the onset of melting. It is shown in this paper that crystal melting and relaxation of the rigid amorphous fraction of PET are largely coupled, and this coupling results in the appearance of multiple endotherms when semicrystalline PET is analyzed by calorimetry.

Overlapping of multiple thermal events in the temperature range where crystals melt was proven for a number of polymers. For isothermally crystallized bisphenol A polycarbonate,[6] poly(3-hydroxybutyrate),[18] isotactic polystyrene,[26] and *cis*-1,4-polybutadiene,[27] it was shown that the small endotherm appearing a few degrees above the crystallization temperature is caused by concurrent partial mobilization of both the crystal and the rigid amorphous fractions. For *cis*-1,4-polybutadiene, which can display up to three major fusion peaks, it was even demonstrated that not only the first endotherm, as seen for other semicrystalline polymers, but also the overall multiple melting behavior is affected by the physical state of the RAF, since it is only in the temperature range of the second major endotherm that the rigid amorphous fraction attains sufficient mobility to allow development of perfected crystals with higher melting point.[27] A similar mutual influence of relaxation of the rigid amorphous segments on the overall multiple melting behavior for PET is proposed and discussed in this contribution on the basis of DSC and TMDSC.

Experimental Part

Material. Poly(ethylene terephthalate) (PET) of molar mass M_w = 21 400 Da was kindly received through the Bank of Crystallizable Polymers of European funded COST Action P12.[28] After drying under vacuum at 100 °C for 16 h, the sample chips were compression-molded with a Carver laboratory press at a temperature of 280 °C for 3 min, without any applied pressure, to allow complete melting. After this period, a pressure of 100 bar was applied for 2 min, and then the sample was quickly cooled to room temperature by means of cold water circulating in the plates of the press.

Calorimetry. The thermal properties of compression-molded PET were measured with a Perkin-Elmer Pyris Diamond DSC, equipped with Intracooler II as cooling system and with a Mettler DSC 822^e calorimeter equipped with a liquid nitrogen cooling accessory. Both the instruments were calibrated in temperature with high-purity standards (indium and cyclohexane) and in energy with heat of fusion of indium. Dry nitrogen was used as purge gas at a rate of 48 mL/min. A fresh sample was used for each analysis in order to minimize thermal degradation. To obtain precise heat capacity data, each measurement was accompanied by an empty pan run and a calibration run with sapphire under identical conditions.[29] All the measurements were repeated three times to improve accuracy.

In order to set the structure for the analysis of melting behavior, each PET specimen of about 4 mg was melted at 280 °C for 3 min and then cooled with 300 °C/min to the crystallization temperature T_c = 190 °C, where it was allowed to crystallize for 30 min. After isothermal crystallization, the PET was cooled with 300 °C/min to 40 °C and then analyzed by heating until complete melting was achieved, using a constant scanning rate of 5 °C/min (Perkin-Elmer Pyris Diamond DSC). The effective cooling rate was not constant down to 40 °C; however, it was sufficient to avoid further crystallization during cooling.

Quasi-isothermal TMDSC data were gained with the Mettler DSC 822^e calorimeter, using a sawtooth oscillation with a temperature amplitude of 0.2 °C and a modulation period of 60 s about a base temperature T_0, which was raised stepwise in temperature increments of 5 °C after 16 min at each T_0. Extended-time quasi-isothermal analyses of duration of 4 h were conducted with the Perkin-Elmer Pyris Diamond DSC at selected temperatures after heating the isothermally crystallized polymer from T_c to T_0 at 5 °C/min. Immediately after completion of the extended-time quasi-isothermal experiments, the DSC was changed to the standard measuring mode and heated from T_0 until complete melting with the scanning rate of 5 °C/min.

From TMDSC measurements the reversing specific heat capacity was obtained from the ratio of the amplitudes of modulated heat flow rate and temperature, both approximated with Fourier series.[30,31] The reversing specific heat capacity values reported in this contribution were obtained from the first harmonics of the Fourier series. Similar to conventional DSC analyses, each TMDSC measurement was accompanied by an empty pan run, and a calibration run with sapphire under identical conditions.[29] The good agreement between the experimental data and the ATHAS Data Bank information proves that the modulation period of 60 s is long enough to be corrected satisfactorily by the calibration with sapphire.

Results and Discussion

Experimental total specific heat capacity (c_p Tot) and quasi-isothermal reversing specific heat capacity (c_p Rev) of PET, measured after isothermal crystallization at 190 °C followed by cooling to 40 °C, are compared in Figure 1 with the thermodynamic c_p of fully solid and liquid PET, as taken from the ATHAS Data Bank.[32] Below the glass transition region and above completion of melting, DSC and TMDSC experimental data agree with the thermodynamic c_p of solid and liquid PET, respectively, as common for PET.[33] The total c_p data reveal a heat capacity step centered around 82 °C, the glass transition temperature (T_g) of the mobile amorphous fraction (MAF), and three main melting endotherms I, II, and III are assigned and numbered in Figure 1 in order of increasing temperatures.

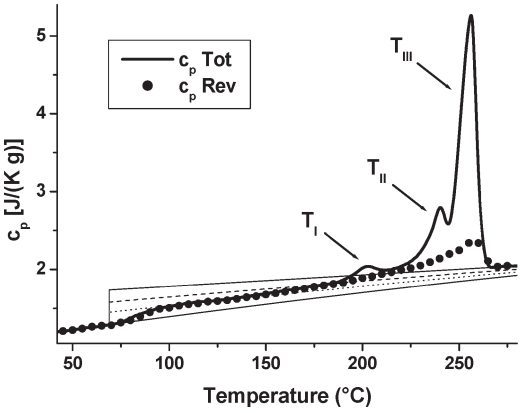

Figure 1. Specific heat capacity of PET after isothermal crystallization at 190 °C and subsequent cooling to 40 °C. The thick solid line is the total heat capacity by standard DSC at 5 °C/min, the solid circles represent the reversing heat capacity after 16 min of modulation at T_0, and the thin solid lines are the solid and liquid specific heat capacities, as taken from the ATHAS Data Bank.[32] The specific baselines heat capacity of PET computed for a two- and three-phase model are shown as dashed and dotted lines, respectively. The major endothermic peaks are numbered in order of increasing temperatures.

The experimental data of Figure 1 allow to determine the three-phase composition of PET. The reference sample, isothermally crystallized at 190 °C for 30 min and cooled, shows a heat capacity step at T_g that accounts for a mobile amorphous phase content (w_A) of 0.36. The crystal fraction as a function of temperature was computed as a first approximation from the conventional DSC plot gained at 5 °C/min by assuming that a two-phase model, consisting of a crystalline and an amorphous fraction, is valid for PET. This working hypothesis involves the assumption either that no rigid amorphous fraction is present in the material or that melting of PET crystals takes place after full devitrification of the RAF. The crystal fraction (w_C) was obtained from eq 1:

$$c_p(T) = w_C(T)c_{p,C}(T) + w_A(T)c_{p,A}(T) - [h_A(T) - h_C(T)]\frac{dw_C(T)}{dT} \quad (1)$$

where $c_p(T)$ is the measured, apparent specific heat capacity, $c_{p,C}(T)$ and $c_{p,A}(T)$ are the thermodynamic values of specific heat capacities of solid and liquid PET, and $[h_A(T) - h_C(T)]$ is the heat of fusion. All thermodynamic data $[c_{p,C}(T), c_{p,A}(T), h_A(T), h_C(T)]$ were taken from the listings in the ATHAS Data Bank.[32] Equation 1 gives a crystallinity $w_C = 0.33_5$. Comparison with the amount of mobile amorphous phase quantified by the heat capacity step at the glass transition suggests considerable rigid amorphous fraction (w_{RA}) under the chosen experimental conditions, $w_{RA} = 0.30_5$. This value is slightly approximated, as in calculation of the crystal fraction devitrification of the RAF in the melting range was not considered, as discussed above. The three-phase composition agrees quite well with the available literature data for PET,[22,25,34−39] although the three-phase structure is affected not only by the specific polymer grade but also by the thermal history of the material.[19,37,40]

An enlargement of the data of Figure 1 around the baseline heat capacities is presented in Figure 2. It reveals that the reversing c_p measured by quasi-isothermal heating crosses the two-phase baseline at 185 °C, suggesting possible complete mobilization of the amorphous segments of PET at this temperature, just before the onset of crystal melting, as postulated in refs 22 and 23. However, some possible reversible melting cannot be excluded, due also to the closeness to the beginning of melting.[23,39]

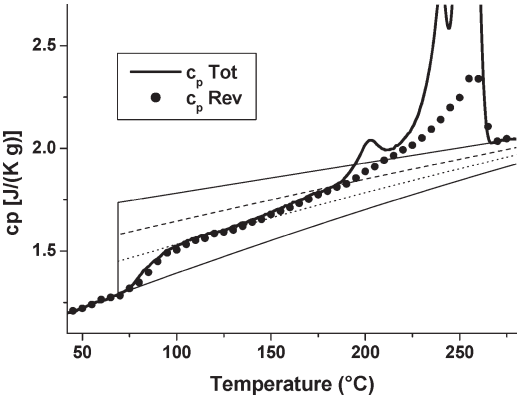

Figure 2. Enlargement of the plot shown in Figure 1 in the area of changing baseline c_p.

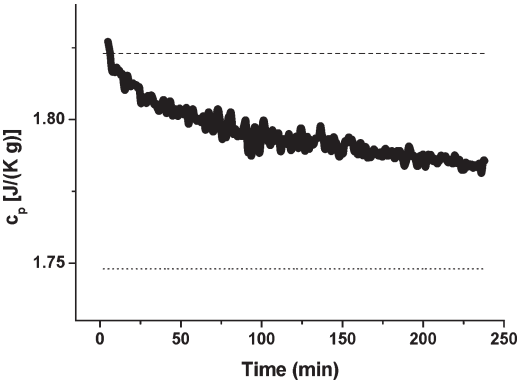

Figure 3. Time dependence of the reversing specific heat capacity of PET during quasi-isothermal TMDSC analysis at 185 °C for 4 h. The specific baseline heat capacity of PET computed for a two- and three-phase model are shown as dashed and dotted lines, respectively.

In other words, the reversing heat capacity measured under quasi-isothermal heating provides information on truly reversible thermal events, like the increase of the baseline heat capacity due to devitrification, but it does not exclude the possible occurrence of other thermal processes involving latent heat exchange that may affect the modulated amplitude of the heat flow rate. The measured apparent, reversing c_p hence may increase up to levels corresponding to a fully mobilized amorphous fraction, caused in part by reversing melting.

In order to determine whether the quasi-isothermal, apparent c_p arises only from thermodynamic heat capacity contributions or contains latent heat effects, the time dependence of the reversing heat capacity at 185 °C was determined. In order to impart the same thermal history of the sample whose thermal analysis is presented in Figures 1 and 2, PET was crystallized at 190 °C for 30 min, then cooled to 40 °C, and subjected to quasi-isothermal step analysis up to the temperature where the reversing c_p intersects the two-phase baseline (185 °C). Then the quasi-isothermal analysis at T_0 = 185 °C was prolonged beyond the 16 min of the previous experiment and extended to 4 h. Results of this analysis, exhibited in Figure 3, reveal that at 185 °C the reversing c_p decays with time and reaches a value of 1.784 J/(K g) after 4 h of quasi-isothermal modulation. This value falls below the baseline heat capacity calculated for a two-phase model that comprises only the crystal fraction and fully mobilized RAF. In fact, it decreases almost to the 50% level of the baseline heat capacity computed using a three-phase model that accounts for the crystal and both mobile and rigid amorphous fractions. The crystal fraction measured by conventional DSC after 4 h of prolonged modulation at 185 °C compares well with the initial

w_C, which indicates that the marked decrease of the apparent c_p seen in Figure 3 cannot be ascribed to an increased crystallinity. Moreover, prolonged annealing of PET might reduce (and not increase) the RAF content, as crystal perfection generally decreases the strain transmitted to the amorphous phase, which excludes the possibility that the decay of apparent heat capacity shown in Figure 3 is caused by an increased amount of solid phases (crystal and rigid amorphous fractions) occurring during the quasi-isothermal modulation at 185 °C. This shows that (i) thermal events involving latent heat exchanges occurring at the crystal surface take place during modulation at 185 °C, as revealed by the decay of reversing heat capacity with time of analysis, a process well investigated for a number of semicrystalline polymers, as reviewed in ref 40; (ii) the intersection of reversing c_p measured by quasi-isothermal step modulation with the baseline heat capacity calculated with eq 1, seen in Figures 1 and 2, is in error since the truly reversible heat capacity at 185 °C has a value lower than measured at short modulation times; and (iii) at 185 °C, immediately before the prior assumed onset of melting, part of the amorphous fraction, that was rigid at completion of the glass transition of the MAF is still vitrified. These observations prove that the RAF becomes mobile in the temperature range of crystal melting, which is about 80 °C wide for PET isothermally crystallized at 190 °C for 30 min.

The existence of a partially vitrified amorphous fraction at the onset of melting of PET crystals is supported by ^{1}H and ^{13}C solid-state NMR analyses discussed in ref 41, which revealed that in a different semicrystalline PET grade subjected to a different (not disclosed) thermal history, somewhat more than 50% of the whole amorphous chains are rigid at 160 °C. The motion in the less mobile amorphous regions identified by solid-state NMR is dominated by rapid, small angular fluctuations that increase in amplitude with temperature. These small-amplitude motions contribute little to the heat capacity beyond the vibrational motion which make up the basic heat capacity of the crystalline and glassy solids.[42] In the RAF at 160 °C, the amplitude of the angular methylene reorientation is greater than that of the aromatic group and is estimated to be in the range 20°−35°, whereas the aromatic ring fluctuations are smaller and are less than 20°. This contrasts with the large-amplitude conformational motions of 120° and 180° which cause the main heat capacity increase in the glass-transition region due to intramolecular and intermolecular potential energy contributions.[42] In the mobile amorphous regions large-amplitude motions of both the methylene and aromatic groups have been quantified, and their rate of motion is ≫100 kHz. The large-amplitude motion within the crystals like the 180° flips of the phenyl rings and interchanges between the *trans*−*gauche* conformational isomers in the −O−CH_2−CH_2−O− chain segments probed by solid-state NMR at 160 °C[41] also contribute to the increases of the measured thermodynamic heat capacity and must be separated from the variation of mobility (and heat capacity) of the amorphous segments.[40] In some crystals of macromolecules such large-amplitude motion leads to mesophase formation or even glass transitions without change of the crystal structure.[40]

The reversing melting, quantified in Figure 3 at 185 °C, can be estimated from the data of Figures 1 and 2 in the whole range of fusion of PET crystals. It has a maximum around 260 °C, as indicated by the quasi-isothermal measurement conducted by modulating around the various base temperatures. More quantitative data were gained by extended-time quasi-isothermal analyses, which were performed by modulating around each base temperature for 4 h after isothermal crystallization at 190 °C, starting from 195 °C and continuing up to complete melting. Results of these analyses are illustrated in Figure 4. For all analyzed temperatures, the reversing c_p plotted vs time displays a double-exponential decay. The reversing c_p after 4 h of modulation at each T_0 and the reversing c_p values extrapolated to infinity are higher that the thermodynamic c_p, indicated by the dotted horizontals.

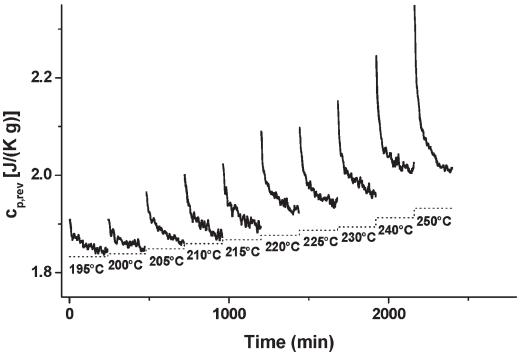

Figure 4. Time dependence of the reversing specific heat capacity of PET during quasi-isothermal measurements at the indicated temperatures. The plots are shifted along the *x*-axis for clarity of presentation. The data are from separate measurements and are collected in a single graph in order to compare the reversing c_p trends for different T_0s. The thermodynamic specific heat capacity of PET is shown as dotted line for each T_0. The crystal fraction used to calculate the thermodynamic c_p was determined by integration of the DSC endotherms gained after the quasi-isothermal analyses.

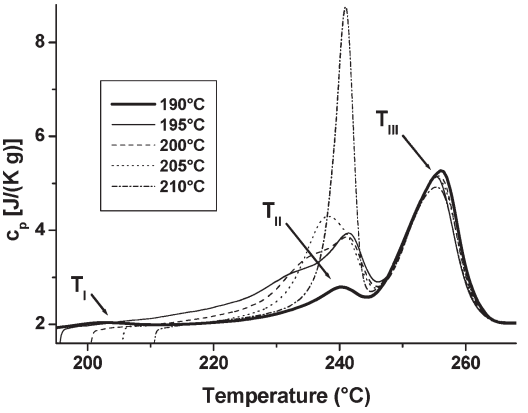

Figure 5. Apparent specific heat capacity of PET measured at 5 °C/min, after isothermal crystallization at 190 °C for 30 min, followed by quasi-isothermal modulations for 4 h at the indicated temperatures, with 195 ≤ T_0 ≤ 210 °C. The thick solid line is the DSC curve at 5 °C/min, after isothermal crystallization at 190 °C for 30 min without quasi-isothermal modulation (as also given in Figures 1 and 2).

Information on the variation of thermal stability of PET crystals upon prolonged exposure at the base temperatures of modulation is provided in Figures 5 and 6, where the experimental apparent heat capacity after 4 h of quasi-isothermal analysis is compared to the c_p vs temperature reference plot of Figure 1 that details the initial structure before prolonged modulation. For clarity of presentation, the experimental data are divided into two separate figures, each for a different range of temperature of the quasi-isothermal treatment.

In Figure 5, the endotherm I at T_I, which appears in Figures 1 and 2 as a separate peak in the reference DSC melting curve, broadens and moves to higher temperatures after 4 h of quasi-isothermal modulation at higher T_0 and produces a shoulder on peak II. The increase with temperature of prolonged quasi-isothermal modulation produces a higher stability of the structure. The location and size of the combined peaks I and II remain little affected by the quasi-isothermal modulation as long as T_0 ≤ 205 °C. A major, abrupt increase in peak size occurs in the DSC curve recorded after 4 h of modulation at T_0 = 210 °C, when the endotherm I at T_I has fully disappeared, and a much narrower

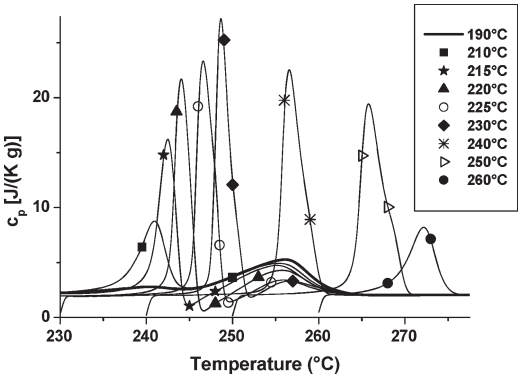

Figure 6. Apparent specific heat capacity of PET measured at 5 °C/min, after isothermal crystallization at 190 °C for 30 min, followed by quasi-isothermal modulations for 4 h at the indicated temperatures, with $210 \leq T_0 \leq 260$ °C. The thick solid line, again, is the specific heat capacity of PET at 5 °C/min, after isothermal crystallization at 190 °C for 30 min without quasi-isothermal modulation (as given in Figures 1, 2, and 5).

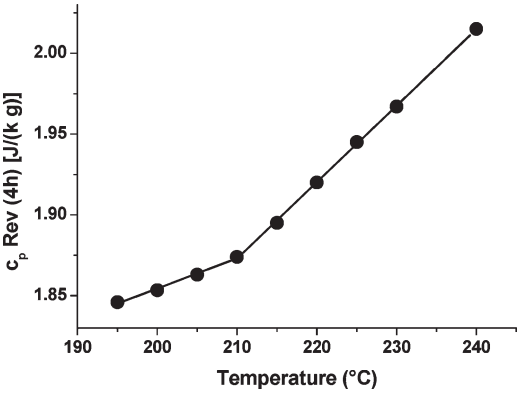

Figure 7. Specific reversing heat capacity of PET after 4 h of quasi-isothermal modulation as a function of the temperature of quasi-isothermal treatment, as shown also in Figure 4.

peak II develops at T_{II}. No noteworthy difference is perceived in the endotherm at T_{III}.

Figure 6 illustrates the thermal analysis of PET after quasi-isothermal modulations of 4 h at $T_0 \geq 210$ °C. After annealing, only two endotherms can be detected in the DSC scans: one at T_{II} and one at T_{III}, as already noted at the high-temperature results of Figure 5. Between $210 \leq T_0 \leq 230$ °C, a rise of temperatures of quasi-isothermal modulation results in a sharper peak II, moved to increasing temperatures. The size and position of the endotherms at T_{III} are also affected by the preceding thermal treatment, and a small intermediate exotherm can be noted between T_{II} and T_{III}, indicative of continuing annealing and recrystallization.[43] Finally, quasi-isothermal modulation at $T_0 \geq 240$ °C results in a single melting endotherm in the DSC. This new, sharper, and larger endotherm IV initially occurs at a temperature $T_{III} = T_{IV}$ and then increases with T_0. The latent heat of the peak IV decreases with increasing T_0.

To make sure the thermal analysis curves illustrated in Figures 5 and 6 are not affected by transesterification processes able to take place during the longtime quasi-isothermal modulations,[44−46] the thermal behavior of PET subjected to prolonged annealing was compared to that of an unannealed sample by repeating the isothermal crystallization for the samples of Figure 6 annealed at 210 and 240 °C. They were melted again at 280 °C for 3 min and recrystallized at 190 °C for 30 min. The DSC melting curves gained at 5 °C/min after this second thermal history were compared to the c_p Tot of nonannealed PET recrystallized at 190 °C for 30 min. No noteworthy difference could be detected between the two sets of PET; hence, the possible effect of ester interchange reactions on the thermal behavior of PET was considered negligible.

The reversing c_p shown in Figure 4 allows to calculate the extent of reversible melting over a wide temperature range. Earlier this was documented for PET only at a few selected temperatures.[23,40] The data are collected in Figure 7 as a function of T_0, the quasi-isothermal temperature of modulation. Two straight lines with different slope intersecting at $T_0 = 210$ °C represent c_p Rev. The DSC data presented in Figures 5 and 6, together with the temperature variation of the reversing heat capacity shown in Figure 7, suggest a change in the reorganization mechanism or kinetics at 210 °C. At the onset of the first endotherm at T_I, the crystals are still coupled to the amorphous phase with chains which are partially vitrified, as shown in Figure 3. A further part of the RAF devitrifies in the temperature range up to 210 °C. As was also demonstrated in ref 25, the endotherm at T_I is, thus, caused by partial mobilization of the rigid amorphous fraction and simultaneous melting of the coupled defective crystals or a degree of order which may be part of the RAF. Such ordered amorphous portions of molecules were observed earlier in drawn polyethylene.[47−49] The rearrangements that occur at T_I may be inhibited not only by constraints exerted by the neighboring crystallites but also by the remaining rigidity in the RAF.[25] As prolonged annealing is conducted at higher temperatures, i.e., up toward the end of the endotherm at T_I of Figures 1 and 2, mobilization of the RAF can allow a higher perfection of the crystals, causing the original endotherm at T_{II}. The melting peak at T_{II} more than doubles in area but does not change in temperature, while the main melting peak at T_{III} is only little influenced by the prolonged stay at $T_0 < 210$ °C. Larger variation in peak shape and positions are observed by modulation at $T_0 \geq 210$ °C, the temperature corresponding to the end of peak T_I. As illustrated in Figure 6, the peak at T_{II} becomes now much sharper and moves to higher temperatures with increasing T_0, whereas the peak at T_{III} gets smaller with little change in temperature. The latter can be explained by considering that the crystals perfected during the quasi-isothermal experiments, whose melting point (T_{II}) is located at higher temperatures, anneal more slowly during the DSC scan than the original crystals. Consequently, they show an exotherm at higher temperature before completing the melting of lesser material which barely reaches the melt end of the reference material analyzed immediately after isothermal crystallization at 190 °C (thick line in Figure 6). An increased stability of PET crystals can be seen in Figure 6 when treated for 4 h at high temperatures (240−260 °C). These higher melting crystals, characterized by their melting peak IV, had annealed and perfected beyond the material treated at lower temperature, melting at T_{III}. They must be lamellae with improved thickness and/or lesser concentration of nonequilibrium defects.

The above results can be rationalized by hypothesizing that at temperatures above 210 °C the constraints in the amorphous phase that do not allow large reorganization of the crystal phase are removed. Literature data indicate that annealing at high temperatures not only may induce crystal perfection and increased crystallinity but also can reduce the rigid amorphous fraction, as documented for cold-crystallized PET and isotactic polypropylene.[37,50] Increased mobility of the strained amorphous segments of PET allows the onset of melting of the coupled crystals that had reached the upper limit of their thermal stability and can now develop more stable structures which ultimately, as melting peaks IV, approach the equilibrium melting temperature (≈280 °C).[32] The sizable variation in the trend of the reversing heat capacity with temperature of quasi-isothermal modulation above or below 210 °C, shown in Figure 7, supports this hypothesis. In the analyzed temperature range, endothermic and exothermic processes that give rise to reversible melting take

place, as evidenced by the values of the reversing heat capacity after 4 h of quasi-isothermal modulation, which are found higher than the specific baseline heat capacity at the corresponding T_0. An increase of the temperature of quasi-isothermal modulation results in a larger crystal fraction that undergoes reversible melting, which, in turn, leads to an increase in the reversing c_p with annealing temperature. The considerable increase in crystal melting point caused by the prolonged exposure at each $T_0 \geq 210$ °C supports the hypothesis that chain mobility is enhanced at $T_0 \geq 210$ °C to levels that permit large extent of recrystallization and crystal perfection which ultimately leads to the melting region IV.

Conclusions

The quantitative thermal analysis of PET presented in this contribution reveals details about the coupling between the crystal and amorphous fractions in PET. Reorganizations of the crystal phase at high temperatures, involving recrystallization/annealing/crystal perfection following partial melting, can occur only if the amorphous segment chains in proximity of the crystal/melt interface have sufficient mobility, which can be achieved upon release of the strain of the amorphous chain segments coupled with the just melted crystals. These results confirm the hypothesis which has appeared in the literature that also in semicrystalline PET the crystal phase must melt, at least partially, before the RAF can become fully mobile.[6,18,27,40] For polymers with a T_g of the RAF above the melting temperature of the crystal, mobilization of the RAF was observed to be needed for crystal melting.[40] In the case of poly(oxy-2,6-dimethyl-1,4-phenylene), the RAF must devitrify first, about 20 °C above T_m, before melting can occur with superheating.[21]

Large coupling between crystal melting and relaxation of the rigid amorphous fraction was also proven for *cis*-1,4-polybutadiene (*cis*-PBD), which, similar to PET, can display up to three major endotherms upon DSC analysis after isothermal crystallization: The whole multiple melting of *cis*-PBD is affected by the RAF, since it is only in the temperature range of the second major endotherm that the rigid amorphous fraction attains sufficient mobility to allow development of perfected crystals with improved thermal stability.[27]

The large degree of coupling between the crystal and the amorphous moieties demonstrated in this contribution for PET cannot be taken as a general rule, as in some polymers no relation between crystal melting and relaxation of the rigid amorphous fraction could be proven. Isotactic poly(1-butene) can be cited as an example where mobilization of the RAF is completed at temperatures well below the onset of melting, thus showing no apparent relation between full mobilization of the amorphous phase with fusion.[19] However, PB-1 crystals (form II) are characterized by large-amplitude intramolecular chain motion, which makes form II polymorph a condis crystal: The high mobility of the crystal phase affects the strain imparted to the amorphous segments coupled to the condis crystals, which favors mobilization of the RAF at low temperatures.[20] These examples underline that dissimilarities exist between the coupling of the crystal and the RAF for the various semicrystalline macromolecules. Each linear macromolecule needs a full characterization to understand the structure−property correlations, as the specific peculiarities of each polymer, coupled with the thermomechanical history, determine its thermal behavior. The combination of DSC, TMDSC, and FSC has proven to be a powerful calorimetric technique to study not only crystals and amorphous polymers but also the multiphase structures with intermediate, coupled nanophases.

References and Notes

(1) Wunderlich, B. *Macromolecular Physics*; Academic Press: New York, 1980; Vol. *3*.
(2) Bassett, D. C.; Olley, R. H.; Al Raheil, I. A. M. *Polymer* **1988**, *29*, 1745–1754.
(3) Xenopulos, A.; Wunderlich, B. *J. Polym. Sci., Part B: Polym. Phys.* **1990**, *28*, 2271–2290.
(4) Cebe, P.; Chung, S. *Polym. Compos.* **1990**, *11*, 265–273.
(5) Wang, Z. G.; Hsiao, B. S.; Sauer, B. B.; Kampert, W. G. *Polymer* **1999**, *40*, 4615–4627.
(6) Sohn, S.; Alizadeh, A.; Marand, H. *Polymer* **2000**, *41*, 8879–8886.
(7) Liu, T.; Petermann, J. *Polymer* **2001**, *42*, 6453–6461.
(8) Kong, Y.; Hay, J. N. *Polymer* **2003**, *44*, 623–633.
(9) Righetti, M. C.; Di Lorenzo, M. L. *J. Polym. Sci., Part B: Polym. Phys.* **2004**, *42*, 2191–2201.
(10) Righetti, M. C.; Di Lorenzo, M. L.; Angiuli, M.; Tombari, E. *Macromolecules* **2004**, *37*, 9027–9033.
(11) Srimoaon, P.; Dangseeyun, N.; Supaphol, P. *Eur. Polym. J.* **2004**, *40*, 599–608.
(12) Di Lorenzo, M. L. *J. Appl. Polym. Sci.* **2006**, *100*, 3145–3151.
(13) Minakov, A. A.; Mordvintsev, D. A.; Schick, C. *Faraday Discuss.* **2005**, *128*, 261–270.
(14) Song, M. *J. Appl. Polym. Sci.* **2001**, *81*, 2779–2785.
(15) Lu, S. X.; Cebe, P. *Polymer* **1996**, *37*, 4857–4863.
(16) Xu, H.; Cebe, P. *Macromolecules* **2004**, *37*, 2797–2806.
(17) Chen, H.; Cebe, P. *J. Therm. Anal. Calorim.* **2007**, *89*, 417–425.
(18) Schick, C.; Wurm, A.; Mohammed, A. *Colloid Polym. Sci.* **2001**, *279*, 800–806.
(19) Di Lorenzo, M. L.; Righetti, M. C. *Polymer* **2008**, *49*, 1323–1331.
(20) Di Lorenzo, M. L.; Righetti, M. C.; Wunderlich, B. *Macromolecules* **2009**, *42*, 9312–9320.
(21) Pak, J.; Pyda, M.; Wunderlich, B. *Macromolecules* **2003**, *36*, 495–499.
(22) Chen, H.; Cebe, P. *Macromolecules* **2009**, *42*, 288–292.
(23) Okazaki, I.; Wunderlich, B. *Macromolecules* **1997**, *30*, 1758–1764.
(24) Schick, C.; Dobbertin, J.; Potter, M.; Dehne, H.; Hensel, A.; Wurm, A.; Ghoneim, A. M.; Weyer, S. *J. Therm. Anal.* **1997**, *49*, 499–511.
(25) Righetti, M. C.; Di Lorenzo, M. L.; Tombari, E.; Angiuli, M. *J. Phys. Chem. B* **2008**, *112*, 4233–4241.
(26) Minakov, A. A.; Mordvintsev, D. A.; Tol, R.; Schick, C. *Thermochim. Acta* **2006**, *442*, 25–30.
(27) Di Lorenzo, M. L. *Polymer* **2009**, *50*, 578–584.
(28) COST P12 ACTION web site: http://www.uni-rostock.de/fakult/manafak/physik/poly/ COST_P12/index.htm.
(29) Archer, D. G. *J. Phys. Chem. Ref. Data* **1993**, *22*, 1441–1453.
(30) Wurm, A.; Merzlyakov, M.; Schick, C. *Colloid Polym. Sci.* **1998**, *276*, 289–296.
(31) Androsch, R.; Moon, I.; Kreitmeier, S.; Wunderlich, B. *Thermochim. Acta* **2000**, *357−358*, 267–278.
(32) ATHAS Data Bank. Pyda, M., Ed.; http://www.prz.rzeszow.pl/athas/databank/intro.html.
(33) Schick, C.; Merzlyakov, M.; Wunderlich, B. *Polym. Bull.* **1998**, *40*, 297–303.
(34) Alsleben, M.; Schick, C. *Thermochim. Acta* **1994**, *238*, 203–227.
(35) Sauer, B. B.; Kampert, W. G.; McLean, R. S.; Carcia, P. F. *J. Therm. Anal. Calorim.* **2000**, *59*, 227–243.
(36) Lin, J.; Shenogin, S.; Nazarenko, S. *Polymer* **2002**, *43*, 4733–4743.
(37) Androsch, R.; Wunderlich, B. *Polymer* **2005**, *46*, 12556–12566.
(38) Righetti, M. C.; Tombari, M.; Angiuli, M.; Di Lorenzo, M. L. *Thermochim. Acta* **2007**, *462*, 15–24.
(39) Androsch, R.; Wunderlich, B. *J. Polym. Sci., Part B: Polym. Phys.* **2003**, *41*, 2039–2051.
(40) Wunderlich, B. *Prog. Polym. Sci.* **2003**, *28*, 383–450.
(41) English, A. D. *Macromolecules* **1984**, *17*, 2182–2192.
(42) See: Wunderlich, B. *Thermal Analysis of Polymeric Materials*; Springer: Berlin, 2005; pp 101−145.
(43) Wunderlich, B. *Thermochim. Acta* **2006**, *446*, 128–134.
(44) Miyagi, A.; Wunderlich, B. *J. Polym. Sci., Part A-2: Polym. Phys.* **1972**, *10*, 1401–1405.
(45) Miyagi, A.; Wunderlich, B. *J. Polym. Sci., Polym. Phys. Ed.* **1972**, *10*, 2073–2083.
(46) Miyagi, A.; Wunderlich, B. *J. Polym. Sci., Polym. Phys. Ed.* **1972**, *10*, 2085–2092.
(47) Kwon, Y. K.; Boller, A.; Pyda, M.; Wunderlich, B. *Polymer* **2000**, *41*, 6237–6249.
(48) Fu, Y.; Chen, W.; Pyda, M.; Londono, D.; Annis, B.; Boller, A.; Habenschuss, A.; Cheng, J.; Wunderlich, B. *J. Macromol. Sci., Phys.* **1996**, *B35*, 37–87.
(49) Chen, W.; Fu, Y.; Wunderlich, B.; Cheng, J. *J. Polym. Sci., Part B: Polym. Phys.* **1994**, *32*, 2661–2666.
(50) Zia, Q.; Mileva, D.; Androsch, R. *Macromolecules* **2008**, *41*, 8095–8102.